JOURNAL OF MATERIALS SCIENCE 29 (1994) 2133–2142

Trapped cracks at indentations

Part I *Experiments on yttria–tetragonal zirconia polycrystals*

R. F. COOK
IBM Research Division, T. J. Watson Research Center, Yorktown Heights, NY 10598, USA

L. M. BRAUN
Ceramics Division, National Institute of Standards and Technology, Gaithersburg, MD 20899, USA

W. R. CANNON
Department of Ceramic Engineering, Rutgers, The State University of New Jersey, Piscataway, NJ 08855, USA

Indentation radial cracking has been examined in a series of yttria–tetragonal zirconia polycrystals (Y–TZP) with a range of grain sizes. For all materials, two distinct types of cracks were found to exist. Above a threshold indentation load, short cracks of variable length were observed, "trapped" in a compressive, contact-induced transformation zone. Above a second threshold, longer, "well-developed" cracks of more consistent length formed, extending beyond the zone boundary. The stochastic nature of the formation of both types of cracks, and the existence of the transformation zone in general, generate many artefacts in toughness estimates made using unmodified indentation fracture mechanics analyses.

1. Introduction

Yttria-doped tetragonal zirconia polycrystals (Y–TZP) can display large values of fracture resistance and strength relative to many ceramics [1, 2]. The large values of these parameters are a consequence of the tetragonal-to-monoclinic phase transformation induced in metastable zirconia grains by the enhanced stress field of a propagating crack. The phase transformation is accompanied by volume and shear strains which act to mitigate the tensile field, leading to an increase in fracture resistance or toughness (an *R*- or *T*-curve). As the transformability depends on the grain-size and the stabilizing yttria-doping level, much effort has been directed towards investigating the influence of these parameters on toughness.

A popular method of estimating toughness has been the measurement of surface traces of cracks generated at indentation contact impressions [3–6]. The method can be used on small "test" volumes of material, and the experiments are quick to perform. However, comparison of indentation results with those obtained using macroscopic test specimens, such as notched beams, can show considerable disagreement. An example of such disagreement is apparent in Fig. 1, which shows toughness as a function of grain size measured by a variety of techniques [7–12]. Similar discrepancies exist in data considering the effect of yttria stabilizer content: indentation techniques suggest different dependencies of toughness on stabilizer content than do macroscopic techniques [11–14].

There are many reasons why indentation techniques may be in disagreement with macroscopic techniques. First, indentation cracks may only sense the "transient", rising part of the *T*-curve, yielding smaller, more variable values of toughness than large cracks sensing the upper, "steady-state" part. This explanation is unlikely, as the scale of the transient region of the *T*-curve in Y–TZP materials is considerably smaller than the indentation crack lengths used [15]. Second, there are many indentation fracture analyses [3–6, 16, 17], involving different assumptions about crack and deformation zone geometry, some of which may not be applicable for a given material. However, while this explanation may account for differences in the absolute magnitudes of estimated fracture resistances (e.g. in the data of Wang *et al.* [11] in Fig. 1), it cannot account for differences in trends (e.g. between the data of Masaki [9], Swain [10], and Wang *et al.* [11]). Third, there are indications that transformation zones occur around indentation impressions in these materials [10, 14,17], adding an additional compressive stress field which is not taken into account in the indentation fracture analyses.

It is the contention of this paper that it is the additional, contact-induced transformation field which is responsible for the discrepancies in both magnitudes and trends between sets of indentation results, and between indentation and macroscopic results. A consequence of a superposition of the compressive transformation field on to the tensile indentation field, with a different magnitude and length-scale,

0022–2461

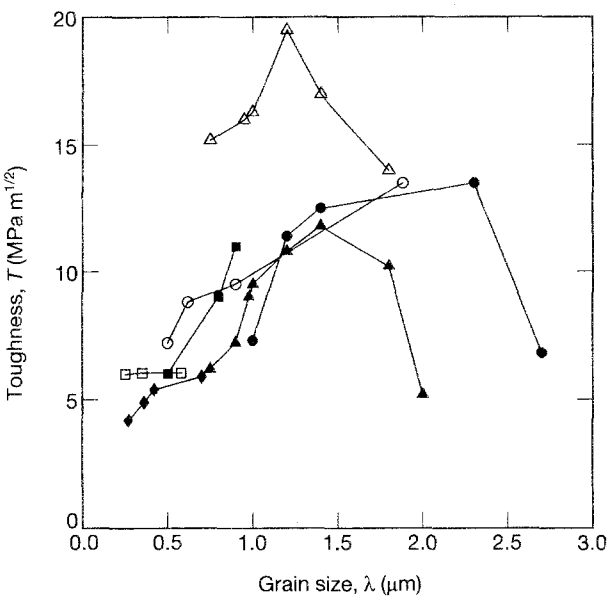

Figure 1 Toughness, T, versus grain size, λ, measured by a variety of techniques for Y–TZP materials: (●) Gao *et al.*, SENB; (○) Swain, IC; (■) Rühle *et al.*, IS; (◆) Braun, CN; (□) Masaki, IC; (▲) Wang *et al.*, IC; and (△) Wang *et al.*, SENB. (IC, indentation crack length; IS, indentation strength; SENB, single-edge notched beam; CN, chevron-notched beam). (●, ○) 2 mol % Y_2O_3; (■, □, ▲, △, ◆) 2.5 mol % Y_2O_3.

is that a new threshold is introduced into the indentation cracking process: in addition to the threshold indentation load necessary for crack initiation, there is now a second, greater threshold load necessary for the formation of "well-developed" cracks. Between these two thresholds cracks remain "trapped" in the transformation field. Failure to distinguish between these two sorts of cracks, or even to account for the retarding influence of the transformation field on well-developed cracks, renders ambiguous all estimates of toughness by indentation techniques.

Here we consider indentation cracking in Y–TZP materials in some detail, demonstrating the threshold effects and the general necessity for including the transformation field into descriptions of indentation cracking in phase-transforming materials. The discrepancies highlighted in Fig. 1 [7–12], in data considering the effects of stabilizer content [11–14], and in the scatter of indentation crack lengths observed in materials with large grain sizes [13], are all seen to arise as a natural consequence of the dependence of the double threshold on the microstructure rather than a dependence of the toughness on the microstructure. We begin with descriptions of the materials preparation and testing procedures. This is followed by presentation of indentation observations and of measurements of the contact impressions, crack lengths, crack probabilities and thresholds. The discussion considers the implication of these results for toughness estimations and comparisons with other zirconia systems. Part II of this series develops a model for the transformation-induced double threshold.

2. Experimental procedure

2.1. Materials

The materials were prepared from a slip of ZrO_2 powder containing 2.5 mol % Y_2O_3 (TZ-2.5Y, Tosoh Corporation, Japan) in distilled water, using ammonium polyacrylic acid (Darvan 821A, R.T. Vanderbilt Company Inc., U.S.A.) as a dispersant and NH_4OH for pH balance. The slip was pressure cast into plates 10 mm thick which were then sintered in air at 1300, 1400, 1500, or 1600 °C for 1 h, to yield samples 98 % dense, with different grain sizes. Specimens were cut from the sintered plates, diamond polished to the 1 μm level, and then annealed at 1250 °C to revert all monoclinic phase arising from the machining and polishing stages to tetragonal phase. X-ray diffraction confirmed the complete reversion to tetragonal [12].

Table I gives the grain sizes, λ, determined from linear intercept counts of scanning electron micrographs of the polished and etched surfaces. Also given in Table I is the toughness, T_∞, determined by chevron-notched-beam tests on specimens cut from the plates [12, 15]. These toughness values characterize the steady-state region of the T-curve appropriate to long cracks with well-developed transformation zones.

2.2. Testing

Specimens were indented with a Vickers diamond pyramid, using peak loads between 5 and 500 N and a dwell time of 15 s. Four to five indentations were made at each chosen load. Contact impression and radial crack surface traces were measured in air by optical microscopy, using bright-field, dark-field, and Nomarski interference contrast. Care was taken to ascertain the ends of the surface traces of the cracks during measurement. No moisture-controlled crack growth was observed. Transformation zones around the contact impressions were observed using Nomarski contrast. Radial crack geometry was determined by serial sectioning of indentations parallel to the specimen surface, and by confirmatory bright-field

TABLE I Properties of Y–TZP materials

Sintering temperature (°C)	Grain size, λ (μm)	Steady-state toughness, T_∞ (MPa m$^{1/2}$)	Hardness, H (GPa)	Well-developed crack parameter, P/l (N μm^{-1})
1300	0.27 ± 0.08	4.2 ± 0.2	12.3 ± 0.5	1.93 ± 0.04
1400	0.36 ± 0.13	4.9 ± 0.1	13.5 ± 0.3	1.78 ± 0.06
1500	0.42 ± 0.15	5.4 ± 0.1	13.4 ± 0.4	1.88 ± 0.03
1600	0.70 ± 0.30	5.9 ± 0.3	12.4 ± 0.3	2.04 ± 0.04

microscopy of fracture surfaces. No lateral cracks were observed in any of the materials over the range of indentation loads used.

3. Results

3.1. Contact deformation and radial crack geometry

Fig. 2 is a Nomarski interference micrograph of a 500 N indentation in the material sintered at 1600 °C. A well-defined square contact impression and surface traces of cracks are clearly visible. Also apparent is an approximately circular contact-induced transformation zone surrounding the contact impression. The zone of contact-induced transformation is approximately twice the diameter of the contact impression (similar to that measured by Lai *et al.* in 2 and 3 mol % Y–TZP [14]), and has an irregular boundary with surface traces of regions disconnected from the central zone. Equally apparent are crack-induced transformation zones adjacent to the crack faces. The crack-induced zones have regular boundaries and the zones are of constant width along the crack length. This last observation indicates that the toughening processes due to the phase transformation have saturated and that the toughness is at its steady-state value, consistent with the observation [15] that the length scale of the transient section of the T-curve in this material is about 30 μm. Although similar transformation zones were not always so readily visible for materials sintered at lower temperatures, the lower steady-state toughness values (Table I), and smaller amounts of monoclinic phase adjacent to cracks (determined by X-ray diffraction [12]), suggest a lower transformability for the smaller grain-size materials, and hence smaller contact-and crack-induced transformation zones.

Fig. 3 is a plot of the contact impression semi-diagonal, a, as a function of indentation load, P, for the four materials. The results for all four materials are

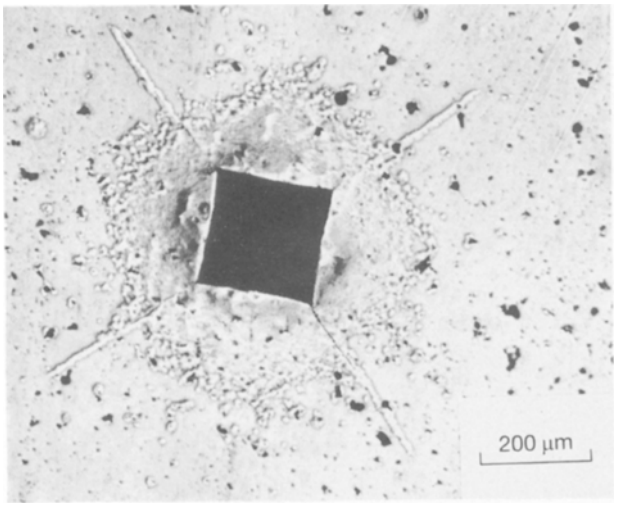

Figure 2 Optical micrograph (Nomarski interference) of a 500 N indentation in the Y-TZP material sintered at 1600 °C. The contact impression with its strain-assisted cooperative transformation zone, and the radial crack traces with their stress-induced toughening transformation zones, are visible.

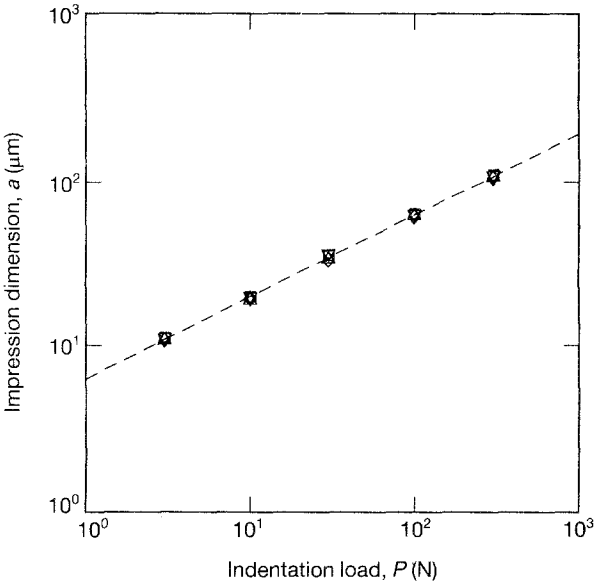

Figure 3 Contact impression dimension, a, versus indentation load, P, for all four Y–TZP materials. The symbols represent the mean of 8–10 measurements, error bars are smaller than the symbol size. (– – –) slope-1/2 best-fit to the data in accordance with Equation 1. Sintered at (▽) 1300 °C, (◇) 1400 °C, (△) 1500 °C, and (□) 1600 °C.

identical and follow the 1/2 power-law dependence consistent with constant hardness, H:

$$H = P/2a^2 \quad (1)$$

The hardness values are given in Table I, and average 12.9 GPa. The load-invariant hardness values suggest that geometrical similarity is maintained in the contact and transformation stress fields, independent of the scale of the contact event (also measured by Lai *et al.* [14]). However, the near-identical values of the hardness observed for the four materials suggests that the contact-induced transformation field is not contributing significantly to the supported contact stress.

The geometry of the cracks was determined as radial, as shown in the optical micrograph of a fracture section, Fig. 4. (We use here the indentation crack notation of Cook and Pharr [18], and distinguish between disconnected radial cracks and connected half-penny cracks.) The cracks have initiated separately at opposite contact-impression edges, not as sub-impression medians. Fig. 4 is similar to previous fracture surface observations on Y–TZP [16, 19, 20], although no tendency to the half-penny geometry at large indentation loads was observed. Scanning electron microscopy suggested that the contrast mechanism of Fig. 4 was due to a greater proportion of transgranular fracture on the radial crack surfaces than on the subsequent failure surface, perhaps associated with a greater proportion of material transformed to monoclinic [21]. To confirm the morphology (i.e. to rule out the possibility that the crack appearance of Fig. 4 is an artefact of the failure process), optical microscopy of serially depth-sectioned indentations was performed, Fig. 5. In Fig. 5a the surface traces of the cracks are clearly detached from the impression corners, indicating that the cracks are not connected under the contact impression. Fig. 5b

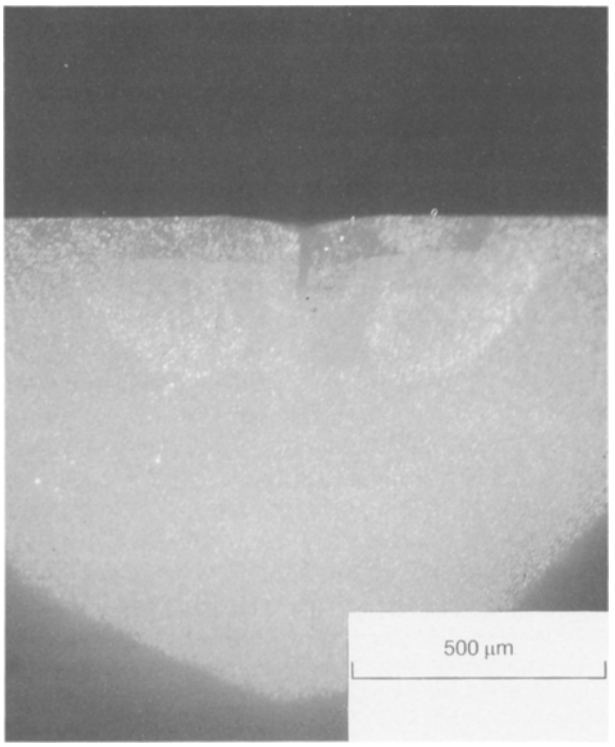

Figure 4 Optical micrograph of the fracture surface at a 500 N indentation site in Y–TZP (1300 °C). The bright areas reveal the traces of disconnected radial cracks initiated at the edges of the contact impression.

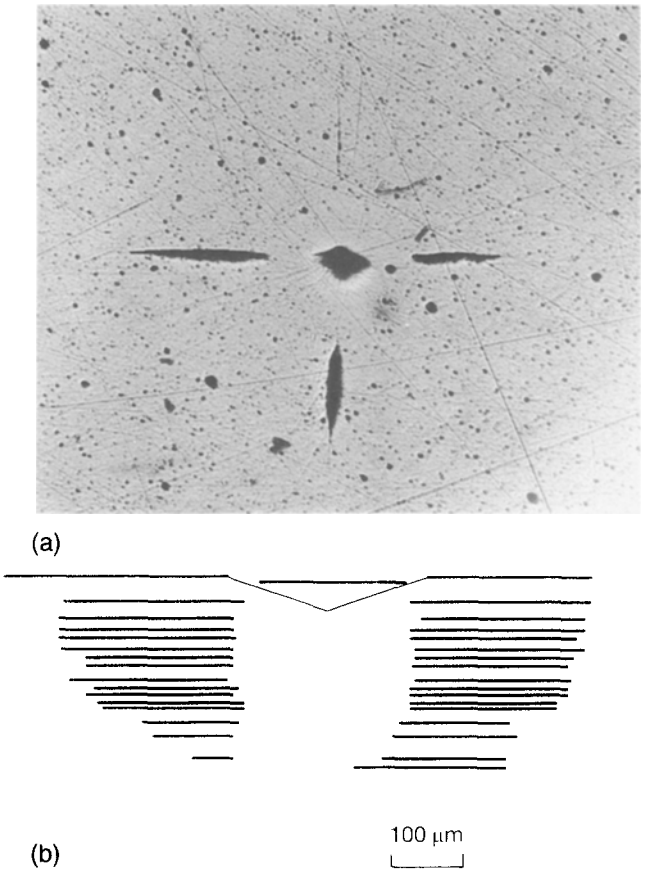

Figure 5 (a) Optical micrograph of a serial section of a 500 N indentation in Y–TZP material (1600 °C), showing crack traces clearly detached from the remnant impression edges. (b) Cross-sectional representation of many such serial sections, confirming the radial crack geometry of Fig. 4. (—) Measured surface traces of cracks at the depths indicated.

shows the results of many sections, confirming the radial morphology. The results of Fig. 5 are similar to other cross-sectional observations on Y–TZP [15, 17] and Ce–TZP [22].

3.2. Radial crack measurements

Figs 6–9 show radial crack-length measurements for the four materials as a function of indentation load. The radial crack length, l, measured from the contact impression corner is used [5, 17, 18, 23]. Four general regions of cracking behaviour were identified, exemplified in Fig. 10:

(i) Below a threshold load no cracking was observed (Fig. 10a).

(ii) Above this load, very short cracks were observed ($l < a$), "trapped" in the contact-induced transformation zone, although not necessarily at every impression corner (Fig. 10b). As the indentation load was increased above this first threshold, radial cracks were observed at more of the impression corners, until, at some larger load, trapped cracks were observed at all impression corners.

(iii) Above a second threshold, longer "well-developed" cracks ($l > a$) formed beyond the transformation zone, in place of the trapped cracks, although again not necessarily at every impression corner (Fig. 10c). Increasing numbers of well-developed cracks were observed as the indentation load was increased above this second threshold.

(iv) Eventually, above a very large indentation load, only well-developed cracks were observed (Fig. 10d).

This last region corresponds to the "classic" indentation region in which indentation fracture mechanics ought to apply. In this case the mechanics

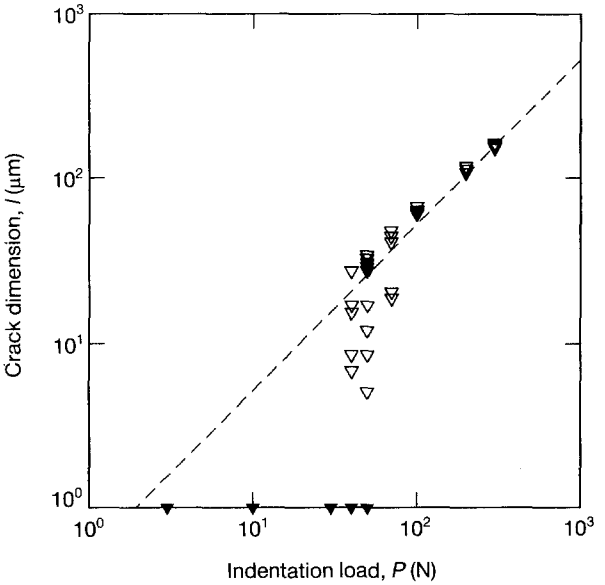

Figure 6 Radial crack length, l, versus indentation load, P, for the Y–TZP material sintered at 1300 °C. Each symbol represents a single crack-length measurement, solid symbols represent completely sub-threshold indentations at which no radial cracks were observed. (– – –) slope-1 fit to the data for the "well-developed" cracks at the largest indentation load, in accordance with Equation 2.

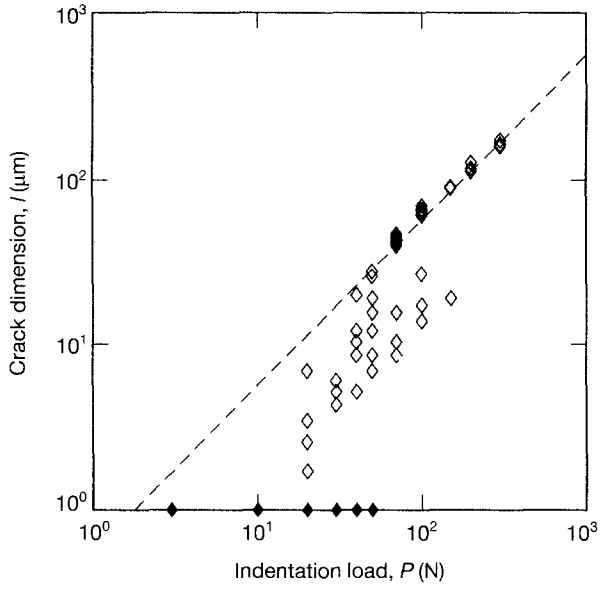

Figure 7 Radial crack length, l, versus indentation load, P, for the Y–TZP material sintered at 1400 °C.

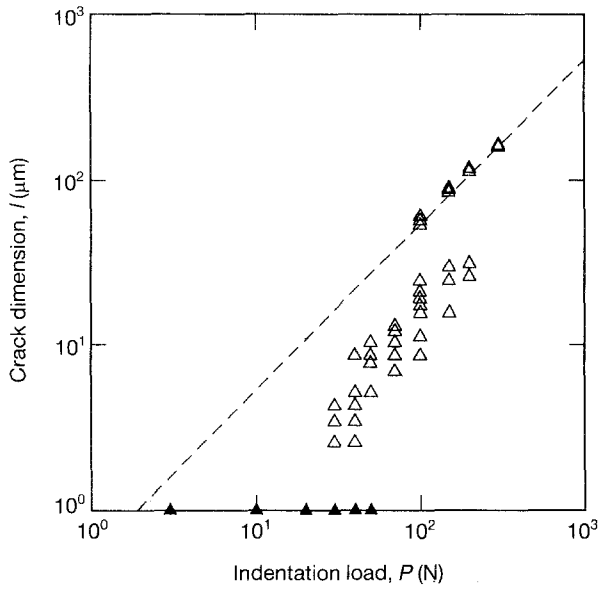

Figure 8 Radial crack length, l, versus indentation load, P, for the Y–TZP material sintered at 1500 °C.

appropriate to radial (or Palmqvist) cracks is used [5], such that the crack length is proportional to the indentation load

$$l = 2\xi^2 E(E/H)^{2/3} P/T^2 \quad (2)$$

where E is the Young's modulus, T the toughness, and ξ a dimensionless geometry parameter characterizing the integrated effect of the stress field acting over the crack. In non-transforming materials, ξ characterizes the contact-induced tensile mismatch field. In zirconia materials, ξ is reduced by the effect of the superposed compressive transformation field; this reduction is different for each material. In non-toughening materials T takes a lower bound value of $T_0 = (2\gamma E)^{1/2}$ characterizing the work of rupture of interatomic bonds. Here, contributions due to transformation toughening increase T with a crack-length dependence

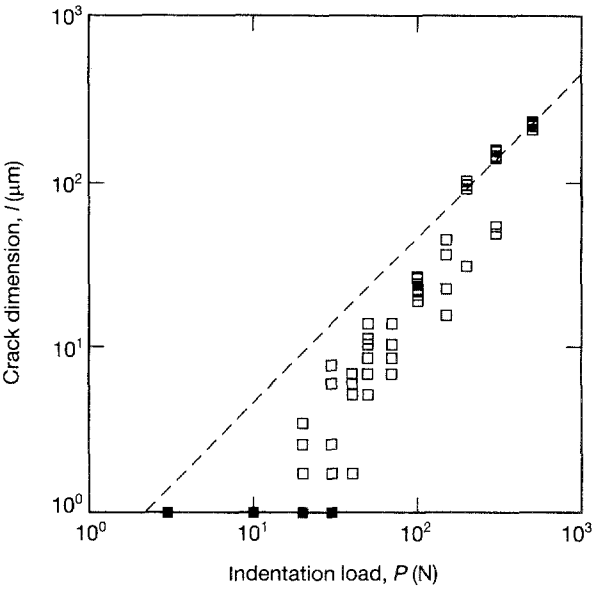

Figure 9 Radial crack length, l, versus indentation load, P, for the Y–TZP material sintered at 1600 °C.

which saturates for long cracks. The well-developed cracks in Figs. 2 and 4–10 are assumed to be in this saturated region such that the value of T in Equation 2 takes the invariant maximum, T_∞. Accordingly, the dashed lines in Figs 6–9 are fits to the data in the well-developed crack region following Equation 2. The values of P/l characterizing these fits are given in Table I. The similar values indicate that the ξ parameters for each material are, in fact, different, although whether this is due to differences in stress-field or crack geometry is difficult to assess. (The crack dimension, c, measured from the centre of the contact impression [4, 18] was also tested, providing $P^{2/3}$-fits to the data for the well-developed cracks, with similar lack of material or geometry discrimination).

To summarize the data of Figs 6–9, Fig. 11 plots the probability of the appearance of a crack as a function of indentation load. The diagonally hatched regions indicate the probability of any crack forming, and the cross-hatched regions indicate the probability of well-developed cracks forming. Clearly, the probability of a well-developed crack forming decreases as the sintering temperature and grain size are increased. This finding is made clear in Fig. 12a which plots the overall probability of cracking as a function of grain size. Although, averaged over the 0–500 N indentation load range (proportional to the area under the curves of Fig. 11) the probability of radial cracking increases slightly with grain size, the probability of forming a well-developed crack decreases significantly. Part of the reason for this is shown in Fig. 12b which is a plot of the threshold loads for cracking, the 0% points in Fig. 11. The lower, dashed line indicates the threshold for any cracking (trapped cracks form first), and decreases slightly with grain size. However, the threshold for well-developed cracks, indicated by the upper, solid line, increases significantly with grain size. The hatched regions above the lines indicate the increases in load required to attain 100% probability

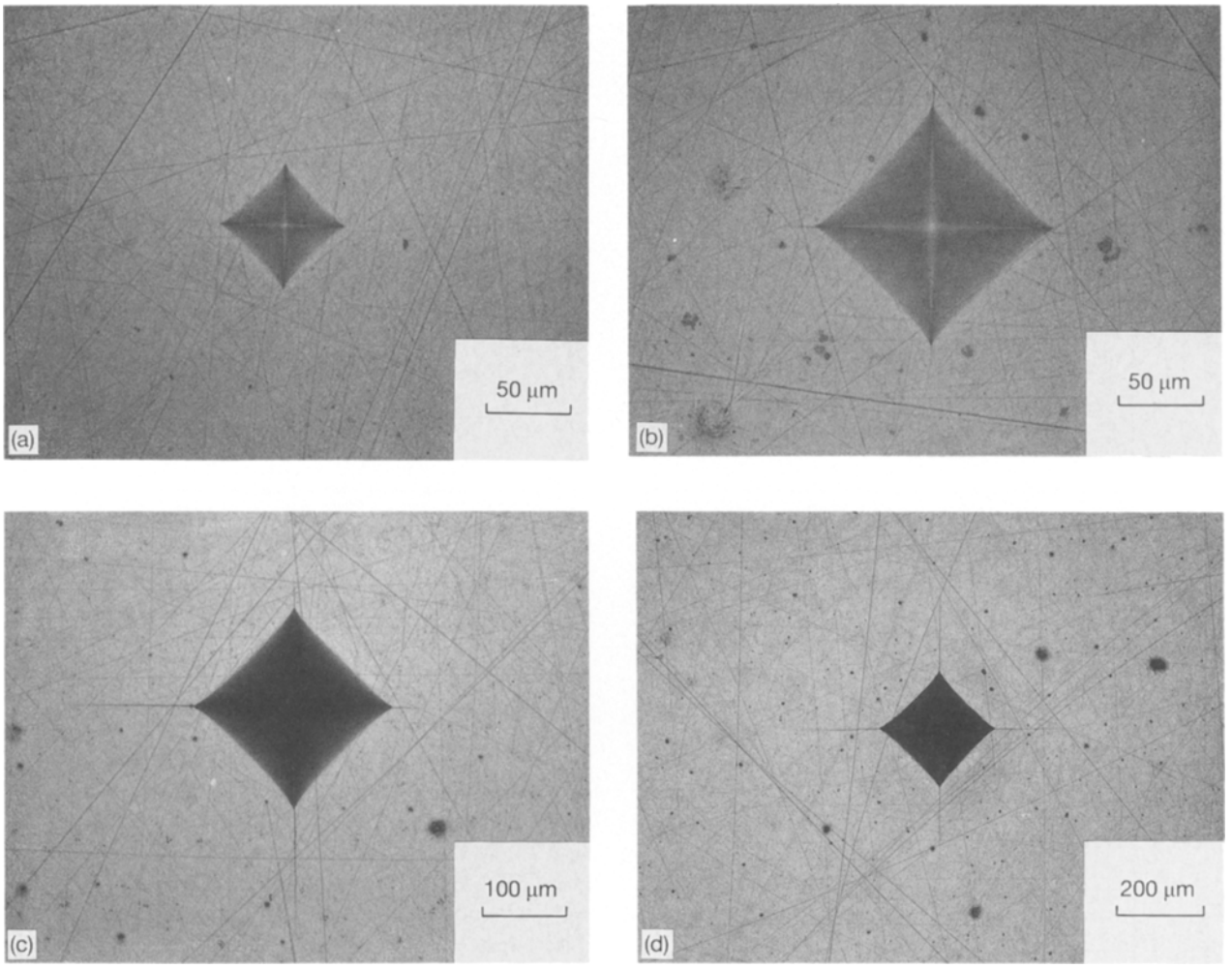

Figure 10 Optical micrographs of indentations in the Y–TZP material sintered at 1500 °C. (a) 20 N indentation load; below the threshold for any radial cracking at the contact impression corners. (b) 70 N indentation load; above the first threshold, for radial cracks "trapped" in the contact-induced transformation zone. (c) 200 N indentation load; above the second threshold, for formation of "well-developed" cracks which have escaped from the transformation zone. (d) 300 N indentation load; above the load required to generate "well-developed" cracks at all impression corners.

for crack generation. These increases diverge with increases in grain size.

4. Discussion

4.1. Implications for toughness estimation

One of the key findings of this work is perhaps best illustrated by estimating the toughness of these materials, deliberately ignoring the obvious effects of the contact-induced transformation zone. Fig. 13 is a plot of toughness as a function of crack dimension from the results of Figs 6–9 and Equation 2, using a value of $\xi = 1.85 \times 10^3$ calibrated from the parameters in Table I for the 1300 °C material and $E = 205$ GPa [1]. The horizontal dashed lines represent the toughness values determined from the chevron-notched-beam tests. Three features are evident. The first is that the apparent toughness decreases with crack length before attaining a steady-state value. Second, the toughness values in the decreasing region are extremely scattered. Third, the apparent toughness in the steady-state region does not agree with the chevron-notch tests for other than the 1300 °C material. It is clear that the simple indentation analysis represented by Equation 2 is not capable of describing the behaviour of a single material, and, even after calibration, does not correlate the responses of the group of materials with independent tests. We consider the reasons for each of the features in Fig. 13 in turn.

The element missing from the analysis is, of course, the effect of the compressive transformation field. Fig. 13 shows that the tendency to decreasing apparent toughness increases with grain size. Lai *et al.* [14] have noted similar decreases in 2 and 3 mol % Y–TZP materials, and explicitly connect the decreases with increasing ratios of crack length to transformation zone-size. The results here support that idea, but only for trapped cracks (i.e. cracks with lengths between 0.1 and 1 times the zone size). The present results are more similar to those of Lai *et al.* for the 2 mol % material, in which the crack lengths varied from 0.7–2 times the zone size. No decrease in apparent toughness is seen here in the well-developed-crack data; this is similar to the relatively invariant toughness result of Lai *et al.* [14] for the 3 mol % material, in which the crack lengths varied from 1.3–3 times the zone size. The implication of both studies is that the more transformable the material (e.g. larger grain size or lower

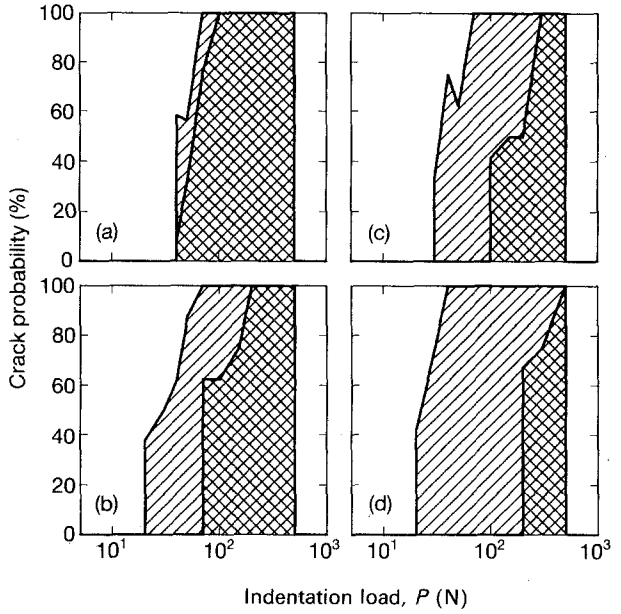

Figure 11 Plot of probability of radial crack formation as a function of indentation load for the four Y–TZP materials. Diagonal hatching indicates all cracks, cross-hatching indicates well-developed cracks. Material sintered at (a) 1300 °C, (b) 1400 °C, (c) 1500 °C, and (d) 1600 °C.

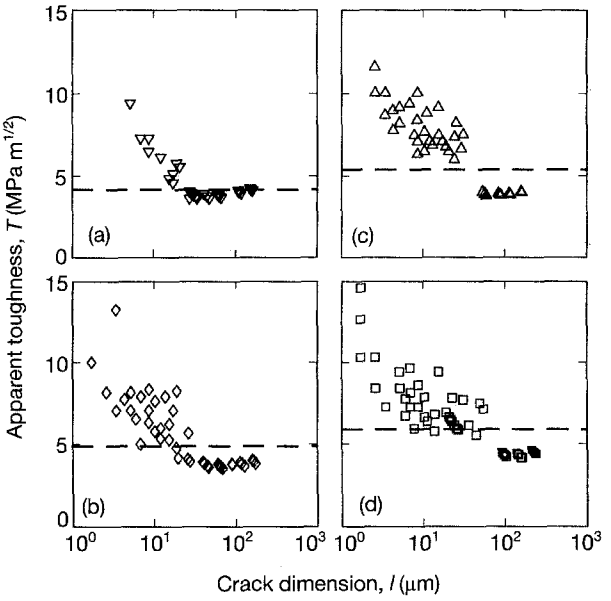

Figure 13 Plot of apparent toughness, T, versus crack dimension, l, for the four Y–TZP materials. The symbols represent individual indentation crack length measurements, (– – –) steady-state toughness determined by chevron notch tests. The decreasing and scattered values at small crack lengths, and the underestimates of the steady-state toughness are all artefacts caused by ignoring the contact-induced transformation zone. (a) Material sintered at 1300 °C, (b) 1400 °C, (c) 1500 °C, and (d) 1600 °C.

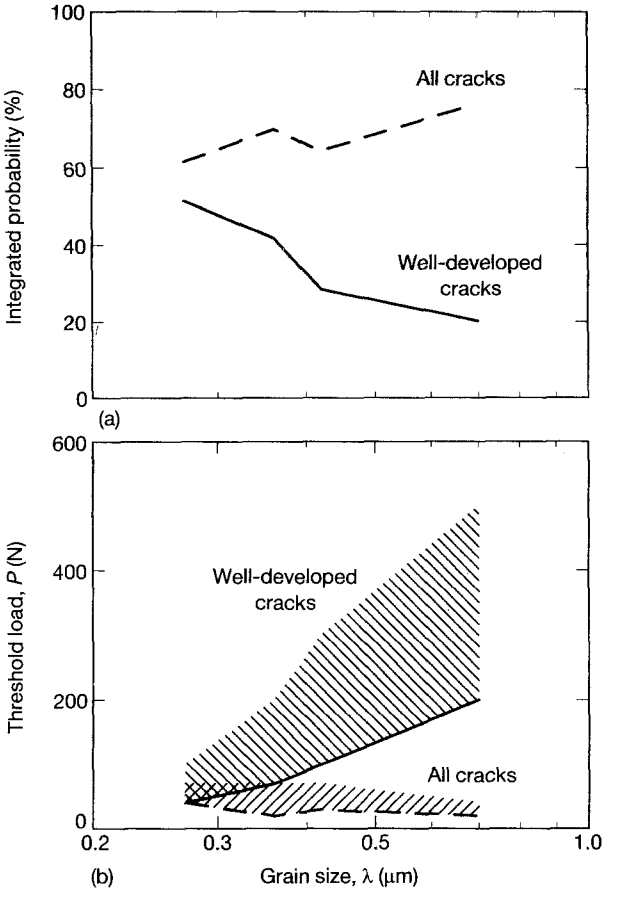

Figure 12 (a) Plot of integrated probability of radial crack formation as a function of grain size for the four Y–TZP materials. Data integrated from Fig. 11 over the 0–500 N load range. (b) Plot of threshold indentation load for radial crack formation as a function of grain size in Y–TZP materials. Data taken from Fig. 11. Lines indicate thresholds for formation of cracks (0% probability in Fig. 11), and boundaries of hatched regions indicate the loads to guarantee crack formation (100% probability in Fig. 11).

stabilizer content) the greater the effect of the contact-induced transformation zone in acting against the mismatch field deriving from the contact event itself.

The transformation-zone effect decreases with increasing crack length for cracks trapped within the zone, before reaching a steady-state value for well-developed cracks. However, Fig. 13 shows that within the zone, the effects can be quite variable, and that trapped cracks can take a wide range of stable lengths. This variation in stable crack length increases with increasing sintering temperature and thus mean grain size and grain-size distribution width (Table I). An interpretation is that as the grain-size distribution increases in relative width, the grain-to-grain transformation probability distribution also increases in width. This increase leads to variability in the transformation zone stress-field and size (the ragged edges and disconnected regions of the transformation zone in Fig. 2 are an example). Hence, the impeding influences of the transformation field will be more variable as the grain-size distribution increases. Such variability is also evident in the increased range of threshold loads for well-developed cracks, Fig. 12b.

The steady-state impeding effect of the transformation zone varies from material to material: more transformable materials yield larger and more compressive zones, which should reduce the lengths of well-developed cracks in the larger grain-size materials. The underestimate of the steady-state toughness by the well-developed indentation crack data in Fig. 13 and Table I suggest, however, that the larger transformation zones are not reducing the crack growth. The implication is that the parameter ξ characterizing the crack geometry, more specifically the surface trace of the radial cracks, cannot be a

constant and must increase with grain size (thus compensating for the longer-than-expected radial crack traces in the larger grain-size materials). Considering the balance between the surface energy and the mechanical energy, the overall crack geometry is thus expected to be shallower and more surface-localized as the grain size and transformability is increased, thereby maintaining the surface trace but decreasing the crack area.

In the light of the above discussion and the results of Figs 6–13, it is hardly surprising that agreement is hard to find between indentation and large crack toughness estimations in Y–TZP materials [7–17]. Grain size, grain-size distribution, stabilizer content, stabilizer segregation, and remnant fractions of cubic and monoclinic phases will all alter the magnitude and scale of the compressive, contact-induced indentation transformation field, thereby altering the *driving force* for fracture *totally independently* from the resisting force or *toughness*. Even if the pitfalls of including variably trapped cracks in the data are avoided, the well-developed cracks are under the influence of a material-dependent impeding force which still renders toughness estimations ambiguous. (Attempts to find a general formulation for indentation cracks in TZP materials [10, 12, 14–17, 19, 22] are essentially attempts to find a compromise value of ξ.)

It is worth noting in this context the similarity between this study and those investigating the effects of lateral cracking on indentation radial crack lengths [23–25]. In both cases, a change in indentation load changes the geometry of the contact event, thereby changing the driving force for radial crack propagation. For lateral cracking the radial-crack driving force is increasingly impeded as the indentation load is increased, thereby increasing the apparent toughness with increasing radial crack length [25]. For contact-induced transformation the radial-crack driving force is decreasingly impeded, thereby decreasing the apparent toughness. Although tendencies to lateral cracking or induced transformation are related to material characteristics to which toughening may also be related, it is important to distinguish between apparent toughness changes mediated by changes in indentation load and thus driving force, and those controlled by crack extension and thus resisting force. Indeed, once the variations in driving force are known, the resistance force may be quantified and material influences on toughness determined [23, 25].

4.2. Comparisons with other systems

Contact-induced transformation zones and the associated suppression of radial cracks have been observed for some time in partially stabilized zirconia (PSZ) systems. Hannink and Swain [26] observed "slip-band"-like surface uplift at Vickers indentations in Ca– and Mg–PSZ, which transmission electron microscopy confirmed as consisting of bands of transformed monoclinic precipitates. Hannink and Swain referred to the contact-induced transformation as "cooperative" because of the localization of the transformed precipitates into bands following the maximum shear-stress trajectories and the discrete shear strains within each band. In the Mg–PSZ material, "peak-aged" to yield maximum transformation and thus toughness, no radial cracking was observed up to 200 N indentation loads, similar to Fig. 10a.

Other studies [27, 28] have shown that "over-aged" Mg–PSZ (which contains very few transformable tetragonal precipitates) generate no cooperative transformation zone, but well-defined radial cracks at Vickers indentations. A similar absence of the transformation zone, with consequent radial cracking, was also observed [27] at Knoop indentations in Mg–PSZ made at 850 °C (at which the tetragonal phase is more stable). Conversely, heat treating "under-aged" Mg–PSZ (in order to render the tetragonal precipitates increasingly metastable and thus transformable) generate larger cooperative transformation zones and smaller or absent radial cracks [29, 30]. Similar suppression of radial cracks in peak-aged material relative to the under- and over-aged conditions has been observed in impact studies on Ca–PSZ [31, 32], and quantified using a crack probability versus contact impression diagram similar to Fig. 11.

In Ce–TZP materials, the cooperative transformation zone is so particularly effective in suppressing radial cracks [22, 33–37] that little study of indentation cracking has been carried out. Hannink and Swain [35] noted an increase in size and raggedness of the cooperative transformation zone with decreasing temperature, as M_s (the martensitic start temperature) was approached, and a total absence of radial cracks. However, below M_s, where no discrete transformation zone could be formed, radial cracks were developed. Tikare and Heuer [36] observed total suppression of radial cracks in Ce–TZP, and also Y–TZP and Mg–PSZ, at 10 N Vickers indentations made below critical temperatures. At indentation temperatures above the critical value, short radial cracks were observed in increasing numbers until, at some greater temperature, longer cracks were observed at all indentation corners. These observations are very similar to those presented in Figs 10–12, with temperature replacing indentation load. Tikare and Heuer also noted that although the contact-impression dimensions were well behaved under given indentation conditions, the crack lengths showed considerable variability. These latter observations are very similar to those presented in Figs 3 and 6–10. The suggestions of Tikare and Heuer were that at the lower, critical temperature conditions for crack nucleation were reached via a dislocation pile-up mechanism, and that above this temperature, crack development was enhanced because of decreasing toughness. An alternative view might be that the conditions for crack *nucleation* within the plastic contact impression were always satisfied, but that above the critical temperature the transformation zone became less effective in impeding crack *initiation* into the surrounding elastic matrix, similar to the Knoop indentations in PSZ [27]. Increasing the temperature further decreases the impeding influence of the transformation zone, leading to longer cracks, even in the absence of any toughness change.

A final comparison may be made with Y–PSZ single crystals [38], heat treated to increase the size of included tetragonal precipitates. Vickers indentations (10 N, aligned to maximize radial cracking [39]) on {100} surfaces of as-grown crystals showed considerable radial cracking. However, annealing the crystals in order to develop the tetragonal precipitates suppressed the radial crack development considerably. In addition, indentations of annealed crystals at elevated temperatures showed increasingly enlarged transformation zones, but no radial cracks. The former observation suggests that at least some part of the cooperative zone is initiated by the plastic deformation in the contact impression, consistent with the "strain-assisted" transformation ideas forwarded for PSZ polycrystals [26, 27].

There are many obvious similarities between the above studies on PSZ, Ce–TZP, and single-crystal materials, and the results presented here on Y–TZP. All support the idea that contact-induced cooperative transformation zones play a dominant role, separate from any toughening considerations, in determining the development of indentation radial cracks. Any factor (e.g. heat treatment) which increases the metastability of the tetragonal phase leads to an increase in the size of the cooperative transformation zone, with an attendant change in the overall stress-field, such that radial cracking is impeded. That the toughening behaviour applicable to any crack may also be increased is a separate issue, similar to the conclusions reached here for Y–TZP.

5. Conclusions

1. Two distinct radial crack populations are generated at indentations in Y–TZP. The first, occurring at low indentation loads, is "trapped" in the contact-induced compressive transformation zone and is short and variable in length. The second, occurring at higher loads, is significantly longer, and is "well-developed" beyond the transformation zone boundary.

2. Threshold loads exist for the appearance of cracks from either population. Between these thresholds, cracks from both populations are generated stochastically.

3. Conventional indentation fracture mechanics does not apply to either population, leading to decreasing, scattered, and improperly calibrated toughness estimates if applied.

4. The observations here and on other TZP and PSZ materials suggest that microstructural changes have two quite separate effects on indentation radial cracking: (i) by altering the "strain-assisted" transformation zone generated by the contact, and (ii) by altering the ability of the material to undergo "stress-induced" transformation toughening.

5. It is emphasized that these conclusions *extend* the usefulness of indentation techniques to characterize material behaviour, rather than limit them, because toughness estimation is made more difficult.

Acknowledgements

The authors thank W. C. Carter, B. R. Lawn, and M. D. Thouless for helpful discussions during the course of the work and reviews of the manuscript. Funding for L.M.B. was partially supplied by the Center for Ceramics Research, Rutgers, The State University of New Jersey, Piscataway, NJ. Certain trade names and products of companies are identified in this paper to specify adequately the materials and equipment used in this research. In no case does such identification imply that the products are necessarily the best available for the purpose or that they are recommended by NIST.

References

1. D. J. GREEN, R. H. J. HANNINK and M. V. SWAIN, "Transformation Toughening of Ceramics" (CRC Press, Boca Raton, 1989).
2. A. H. HEUER, F. F. LANGE, M. V. SWAIN and A. G. EVANS, *J. Am. Ceram. Soc.* **69** (1985) i.
3. A. G. EVANS and E. A. CHARLES *ibid.* **59** (1976) 372.
4. G. R. ANSTIS, P. CHANTIKUL, B.R. LAWN and D. B. MARSHALL, *ibid.* **64** (1981) 533.
5. M. T. LAUGIER, *ibid.* **68** (1985) C-51.
6. C. B. PONTON and R. D. RAWLINGS, *Mater. Sci. Technol.* **5** (1989) 865.
7. M. RÜHLE, N. CLAUSSEN and A. H. HEUER, in "Science and Technology of Zirconia II", edited by N. Claussen, M. Rühle and A. H. Heuer (American Ceramic Society, Columbus, OH, 1984) p. 352.
8. L. GAO, T. S. YEN and J. K. GUO, in Science and Technology of Zirconia 3, edited by S. Somiya, N. Yamamoto and H. Hanagida, (American Ceramics Society, Westerville, OH, 1988) p. 405.
9. T. MASAKI, *J. Am. Ceram. Soc.* **69** (1986) 638.
10. M. V. SWAIN, *J. Mater. Sci. Lett.* **5** (1986) 1159.
11. J. WANG, M. RAINFORTH and R. STEVENS, *Br. Ceram. Trans. J.* **88** (1989) 1.
12. L. M. BRAUN, PhD thesis, Rutgers University (1990).
13. F. F. LANGE, D. B. MARSHALL and J. R. PORTER, in "Ultrastructure Processing of Advanced Ceramics", edited by J. D. MacKenzie and D. R. Ulrich (Wiley, New York, 1988) p. 519.
14. T. R. LAI, C. L. HOGG and M. V. SWAIN, in "Ceramic Developments", edited by C. C. Sorrell and B. Ben-Nissan (Trans Tech, Switzerland, 1988) p. 1071 (also in *Trans. Iron Steel Inst. Jpn* **28** (1989) 240).
15. R. M. ANDERSON and L. M. BRAUN, *J. Am. Ceram. Soc.* **73** (1990) 3059.
16. G. ORANGE, K. M. LIANG and G. FANTOZZI, in "Science of Ceramics", Vol. 14 edited by D. Taylor (Institute of Ceramics, Stoke-on-Trent, 1988) p. 709.
17. J. C. GLANDUS, T. ROUXEL and Q. TAI, *Ceram. Int.* **17** (1991) 129.
18. R. F. COOK and G. M. PHARR, *J. Am. Ceram. Soc.* **73** (1990) 787.
19. S. L. JONES, C. J. NORMAN and R. SHAHANI, *J. Mater. Sci. Lett.* **6** (1987) 721.
20. S. AKIYAMA, Y. KIMURA and M. SEKIYA, *J. Soc. Mater. Sci. Jpn* **38** (1989) 1415.
21. S.-Y. CHEN and H.-Y. LU, *J. Mater. Sci.* **23** (1988) 1195.
22. R. K. MATSUMOTO, *J. Am. Ceram Soc.* **70** (1987) C-366.
23. R. F. COOK and E. G. LINIGER, *J. Mater. Sci.* **27** (1992) 4751.
24. R. F. COOK and D. H. ROACH, *J. Mater. Res.* **1** (1986) 589.
25. R. F. COOK, M. R. PASCUCCI and W. H. RHODES, *J. Am. Ceram Soc.* **73** (1990) 1873.
26. R. H. J. HANNINK and M. V. SWAIN, *J. Mater. Sci.* **16** (1981) 1428.
27. R. H. J. HANNINK and M. V. SWAIN, in "Deformation of Ceramics II", edited by R. E. Tressler and R. C. Bradt (Plenum, New York, 1984) p. 695.
28. D. B. MARSHALL, *J. Am. Ceram Soc.* **69** (1986) 173.
29. M. V. SWAIN, *Acta Metall.* **33** (1985) 2083.
30. D. B. MARSHALL and M. V. SWAIN, *J. Am. Ceram Soc.* **71** (1988) 399.

31. H. P. KIRCHNER, R. M. GRUVER, D. M. RICHARD and R. C. GARVIE, *Mater. Sci. Eng.* **40** (1979) 49.
32. H. P. KIRCHNER and T. J. LARCHUK, in "Fracture Mechanics of Ceramics", Vol. 6, edited by R. C. Bradt, A. G. Evans, D. P. H. Hasselman and F. F. Lange (Plenum Press, New York, 1983) p. 327.
33. K. -H. HEUSSNER and N. CLAUSSEN, *J. Eur. Ceram. Soc.* **5** (1989) 193.
34. Y. L. CHEN and R. J. BROOK, *Br. Ceram. Trans. J.* **88** (1989) 7.
35. R. H. J. HANNINK and M. V. SWAIN, *J. Am. Ceram. Soc.* **72** (1989) 90.
36. V. TIKARE and A. H. HEUER, *ibid.* **74** (1991) 593.
37. D. B. MARSHALL, J. J. RATTO and F. F. LANGE, *ibid.* **74** (1991) 2979.
38. J. MARTINEZ-FERNANDEZ, M. JIMENEZ-MELENDO, A. DOMINGUEZ-RODRIGUEZ and A. H. HEUER, *ibid.* **74** (1991) 1071.
39. A. PAJARES, F. GUIBERTEAU and A. H. HEUER, *ibid.* **74** (1991) 859.

Received 19 April
and accepted 16 August 1993.